Detonation Diffraction

J.E. Shepherd, E. Schultz, R. Akbar*

Graduate Aeronautical Laboratories, California Institute of Technology, Pasadena, CA 91125, USA.

Abstract: We contrast the problems of detonation and shock diffraction over convex and concave corners. Detonations are distinguished from shock waves by the presence of an intrinsic length scale associated with a reaction zone. The extent of this reaction zone depends on both the nature of the chemical system and the detonation wave speed. The dependence of the reaction front thickness on wave speed causes the diffraction of detonations to be essentially different from shock waves. Shock waves diffract in a self-similar manner around both concave and convex corners, but detonations do not. The departure of detonations from self-similarity is manifested most dramatically in diffracting around convex corners. Under certain conditions, a detonation can fail by degenerating into a weak shock followed by a low-speed flame. Diffraction around concave corners also departs from self-similarity but the behavior is bounded by the limits of frozen and equilibrium flow.

Key words: detonation, diffraction, Mach reflection

1. Introduction

The study of shock wave diffraction (Hornung 1985, Skews 1967) is greatly simplified by the use of similarity solutions. This is possible when there are no length scales introduced by either the geometry or physical processes within the shocked gas. As long as the shock layer structure is unimportant on the scale of the experiment (Hornung and Smith 1979), often the case in many shock tube studies of diffraction, self-similar behavior is evident as shown in Fig. 1.

In the case of detonations, an intrinsic length scale is always present due to the intense chemical reactions that occur in a layer just behind the leading shock wave (Fig. 2). The thickness Δ of the reaction zone is a function of the chemical system and the proportions of fuel and oxidizer as illustrated in Fig. 3 for the hydrogen-oxygen and hydrogen-air system. A second length scale λ is created as a result of the nonlinear coupling between the chemicial reaction rates and the gas dynamics that creates a turbulent structure on and behind the detonation front. The nature of the turbulent structure is shown in Fig. 4 as manifested in a shadowgraph (a) and on sooted foils (b) placed against the inside tube wall. An idealized sketch of the front structure is shown in Fig. 4c, illustrating how the triple point tracks create the cellular pattern with characteristic spacing λ on the sooted foil. The length λ is between 10 and 100 times the computed idealized reaction zone length depending on the chemical system.

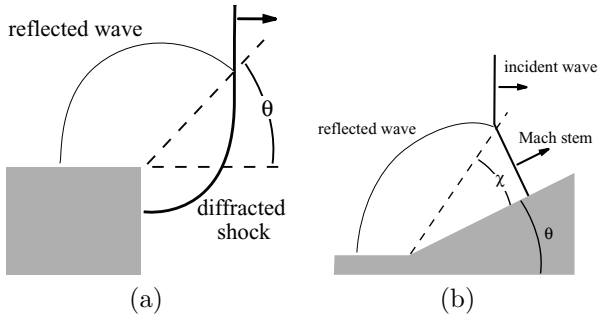

Figure 1. Shock waves exhibit self-similar or conical flow behavior during diffraction over sharp convex (a) and concave (b) corners. The flows are characterized by angles that are a function of the incident shock Mach number.

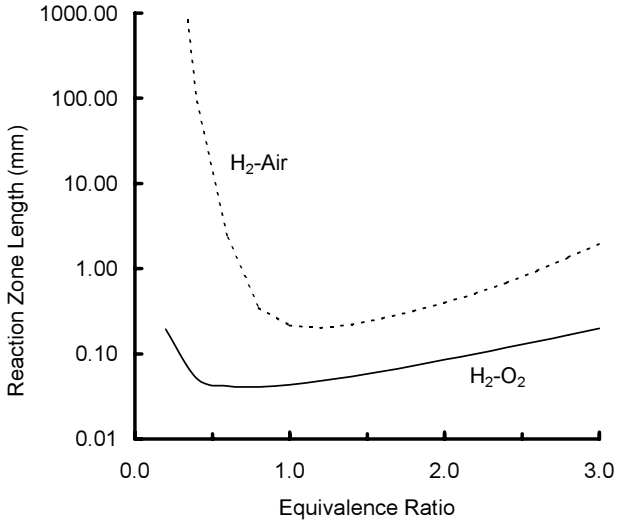

Figure 3. Computed idealized reaction zone thickness for detonations in hydrogen-oxygen and hydrogen-air mixtures propagating at the Chapman-Jouguet (CJ) velocity (295 K and 1 bar).

In addition to the intrinsic chemical length scale, detonations have a length scale associated with the expansion wave (Taylor-Zeldovich wave) flow immedi-

*Present address: Combustion Dynamics Ltd, Medicine Hat, Alberta, CANADA

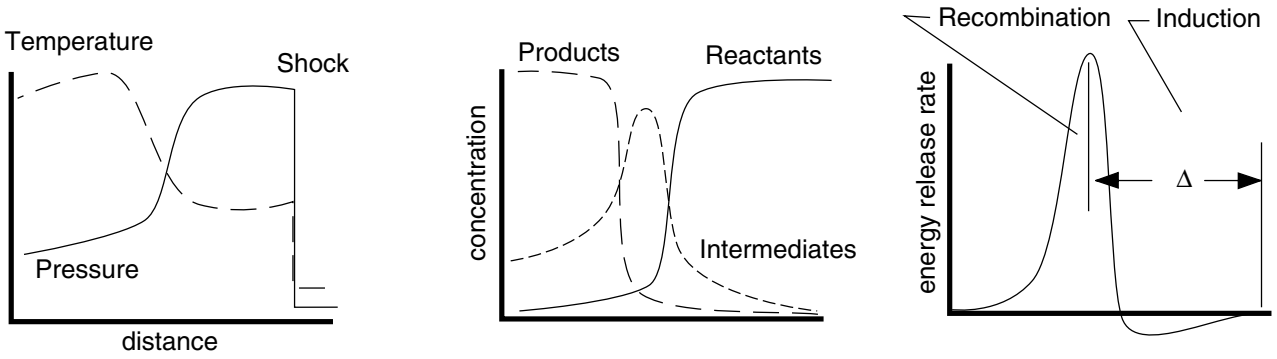

Figure 2. Idealized reaction zone structure in detonations.

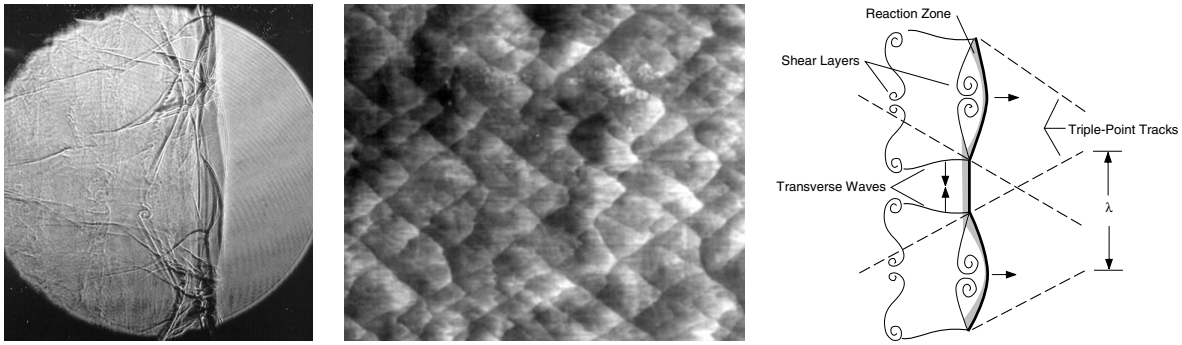

(a) (b) (c)

Figure 4. Cellular structure of detonation fronts. (a) shadowgraph visualization. (b) soot foil tracks. (c) schematic of front structure.

ately behind the detonation front. Unlike shock waves, in which it is relatively easy to generate a uniform flow behind the shock front, detonations almost invariably are generated in a fashion that results in nonuniform flow. The characteristic length L associated with the Taylor-Zeldovich flow for planar waves is about one-half the propagation distance from the origin of the detonation wave. In the cases of interest for our study, the detonations have propagated several meters from the initiator, which is usually a factor of 10 to 100 times larger than the observation length of a few centimeters associated with the gradients produced by diffraction. For this reason, we focus on the role of flow gradients associated with the diffraction process rather than the initiation process.

1.1. Failure of Self-similarity

The effect of all of these length scales, $\Delta < \lambda < L$, is to spoil the possibility of a unique self-similar solution for diffraction of detonation waves. The results of any experiment have to be analyzed considering the thickness of the front relative to the characteristic physical length scale ℓ over which the measurements are taken. From an experimental viewpoint, the appropriate thickness measure of the front is the cell width λ while most theoretical considerations use the idealized reaction zone thickness Δ. For diffraction over sharp corners, the observation length scale is that associated with the wave transit time, $\ell \sim Ut$, from the corner itself.

Studies on shock waves in dissociating gases (Hornung and Smith 1979) have identified two limiting regimes in which self-similar behavior will be recovered. The frozen limit, $\lambda/\ell \to \infty$, will occur at early times and the diffraction process is controlled by nonreactive or "frozen" dynamics of the leading shock front. The equilibrium limit, $\lambda/\ell \to 0$, will occur at late times and the diffraction process is controlled by fully-reacted or "equilibrium" dynamics of an idealized, thin reaction front. Although this classification seems reasonable to extend to detonations, this simple picture is complicated by the dependence of the reaction zone thickness on the strength of the leading shock front. The outcome of a diffraction experiment with a detonation can be dramatically different from the diffraction of a shock wave in a dissociating gas since the speed of the detonation wave depends on the coupling of the reaction zone to the shock front. Decoupling of the reaction zone from the shock front can cause the propagation mode to change from a detonation traveling at 3000 m/s to a sound wave followed by a subsonic flame.

We have systematically explored these two regimes through experiments; varying the characteristic length λ by changing the amount of diluent and the initial pressure in the reactants. This is not a new subject (Bazhenova et al. 1965, Edwards et al. 1979, Gavrilenko and Prokhorov 1983, Zeldovich et al. 1956) but previous work is often contradictory since the role of the intrinsic length scale has not always been explicitly recognized. We have recently carried out high-resolution flow visualization studies in our laboratory (Akbar 1997, Schultz 1998) to examine some quantitative aspects of the diffraction process. Some preliminary results for the cases of Mach reflection and corner turning are given below.

2. Mach Reflection

The effect of the chemical reaction length scale on detonation Mach reflection is shown in Fig 5. The key difference between shocks and detonation waves is the horizontal striations appearing behind the detonation wave. These striations, either shock waves or contact surfaces, are evidence of the weak transverse shock waves propagating along the main front. The interaction of the transverse waves with the main reflected wave is one of the essential differences between shock and detonation diffraction. This results in a blurring of the main triple point location and makes it difficult to distinguish the associated reflected wave and contact surface. Note that the cellular wave spacing is smaller behind the Mach stem than the incident wave. This is a consequence of decreasing reaction zone length with increasing wave speed.

The reflection of shock waves from two-dimensional wedges was systematically explored (Akbar 1997) for wedge angles between 15° and 50°. The effect of cell width λ and the regularity of the cellular structure was examined for three mixtures, given in Table 1. Some representative results are given for two wedge angles in Fig. 6. The first row of shadowgraphs is for a wedge angle of 20°, much less than the critical angle of about 40° for transition from Mach to regular reflection, shown in the second row of images. The triple point and reflected wave features in the 40° case are much more distinct at 40° than at 20° since the Mach stem is much stronger. Images (a), (b), (d) and (e) have incident wave cell widths of 7-15 mm, comparable to or larger than the Mach stem height shown. The third image (c) has incident cell widths of 1-2 mm, smaller than the Mach stem height. A secondary effect is that the cellular structure of the highly Ar-diluted mixtures is very regular in comparison to the undiluted mixture.

Detailed analysis of the wavefront shapes and trajectories is not completely consistent with either the frozen or equilibrium limits. This is most evident when the main triple point track trajectory angle χ (see Fig. 1) is plotted vs. wedge angle θ and compared to the results of model computations for the limiting cases of frozen and equilibrium interactions (Akbar 1997). The first method used the three-shock construction (assuming the Mach stem is straight and normal to the surface of the ramp) and matched the flow deflection angle across the contact surface (Hornung 1985) using numerical solutions with realistic thermochemistry for the gases. The second method used the approximate shock dynamics method of Whitham, appropriately modified for detonations (Akbar 1991). The present results are shown in Fig. 7 for all three mixtures. The mixture ($2H_2$+O_2+10.33Ar, 20 kPa) with the largest cell width λ appears to be close to the frozen flow limit. The mixture (C_2H_2+$2.5O_2$+14Ar, 50 kPa) with the smallest cell width appears to be near equilibrium for large wedge angles but intermediate at smaller values. The mixture ($2H_2$+O_2, 20 kPa) appears to be closest to equilibrium although it has a cell width of 7-8 mm. The irregular nature of the cellular structure of this mixture may be a factor. Note the lack of data for wedge angles less than 20°, a region where the difference between predicted equilibrium and frozen behavior is quite pronounced. It is difficult to obtain data at smaller wedge angles since the wave fronts were curved near the triple point making the location ambiguous; also, the reflected wave is weak and obscured by the transverse waves.

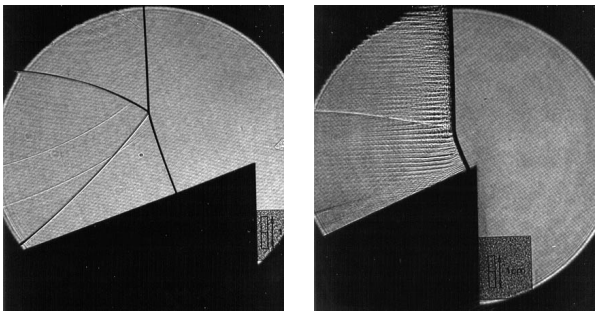

(a) (b)

Figure 5. Shadowgraph visualization of the diffraction of (a) shock wave (M=1.7, air) on a 20° wedge and (b) detonation in Ar-diluted acetylene-oxygen mixture on a 25° wedge (Akbar 1997).

In Fig. 7c, we compare the $2H_2$+O_2 mixture with the previous results (Meltzer et al. 1993) obtained using soot foils. At 20° the values of χ inferred from the soot foils are significantly higher than from the shadowgraphs. At 25° and 30°, the data from the soot foils are slightly higher than from the images. In addition, we can see from the images that the trans-

Mixture	P_0 (kPa)	U_{CJ} (m/s)	λ (mm)	Structure
$2H_2 + O_2$	20	2757	7 - 8	irregular
$2H_2 + O_2 + 10.33$ Ar	20	1540	15 - 18	regular
$C_2H_2 + 2.5\ O_2 + 14.0$ Ar	50	1688	1.75	regular

Table 1. Mixture properties for Mach reflection study (Akbar 1997)

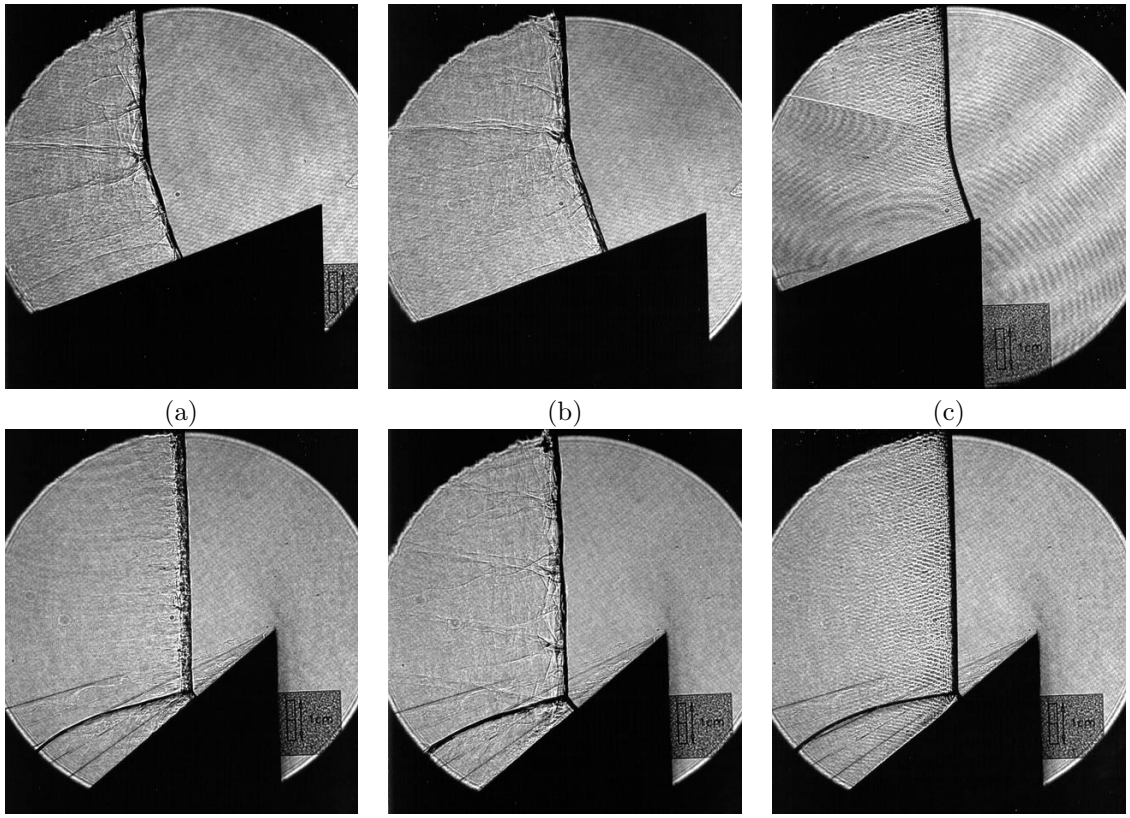

Figure 6. Detonation Mach reflection on a 20° wedge: (a) $2H_2$+O_2, 20 kPa. (b) $2H_2$+O_2+10.33Ar, 20 kPa. (c) C_2H_2+2.5O_2+14Ar, 50 kPa. On a 40° wedge: (d) $2H_2$+O_2, 20 kPa. (e) $2H_2$+O_2+10.33Ar, 20 kPa. (f) C_2H_2+2.5O_2+14Ar, 50 kPa. (Akbar 1997)

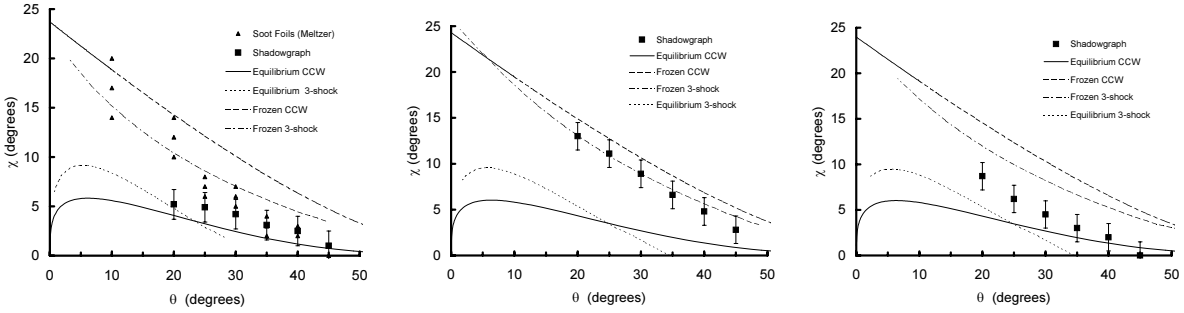

Figure 7. Triple-point trajectories inferred from laser schlieren photographs and compared to simple models of the reflection process. (a) $2H_2$+O_2, 20 kPa. (b) $2H_2$+O_2+10.33Ar, 20 kPa. (c) C_2H_2+2.5O_2+14Ar, 50 kPa.(Akbar 1997).

verse waves may propagate through the Mach reflection triple point so that changes in cell width may not be truly indicative of the main triple point location. This is a particular problem with irregular

mixtures and weak reflected waves for which it is difficult to distinguish on the sooted foil the Mach reflection triple points from the instability wave triple points. All this suggests caution is in order when interpreting sooted foils in this type of experiment. The cases studied are not close enough to the limiting situations to provide definite tests of the frozen and equilibrium limits although it is clear we have approached those limits in some instances. The available data is bounded by the equilibrium and frozen limits. Future experiments should include consideration of the reaction length scale in analyzing detonation Mach reflection.

3. Corner Turning

The breakdown of self-similarity and the influence of the reaction zone length scale is much more striking in diffraction around convex corners. Examples can be seen in Fig. 8, a detonation diffracting about a corner created by a tube emerging into a larger volume. The dependence of reaction layer thickness on shock strength can result in the catastrophic increase of reaction zone thickness when the leading shock weakens as it diffracts out of the tube into the surrounding region. In Fig. 8a, a region of shocked but unreacted gas can be seen behind the shock front in the vicinity of the tube opening. A highly disturbed region near the front results from the reinitiation of the detonation. High-speed movies show that this region spreads from the front to the rear of the wave, reinitiating the detonation process along the entire wave front. Experimental observations (Bazhenova et al. 1965, Edwards et al. 1979, Zeldovich et al. 1956) show that the outcome of the diffraction process depends on the ratio of the reaction zone thickness or cell width to the tube diameter and also, the specifics of the chemical system. A general rule of thumb is that when $D < A\lambda$, reinitiation of the detonation wave does not occur and a shock wave followed by a contact surface is the final result. The constant A is between 10 and 30 depending on the shape of the opening and the type of mixture (Shepherd et al. 1986). The extremes of the behavior observed in initiation are shown in photographs (b) and (c) of Fig. 8. These two shadowgraphs illustrate the subcritical (b) and supercritical (c) situations that bracket the critical case (a).

The origin of the dramatic behavior shown in Fig. 8 is the strong dependence of the reaction time on the shock strength. Estimates of reaction time for the stoichiometric hydrogen-oxygen system are shown in Fig. 9. Note the extremely rapid increase of reaction time with decreasing shock strength below a shock speed of $0.8U_{CJ}$. This is due to the Arrhenius dependence of reaction rates on postshock temperature and

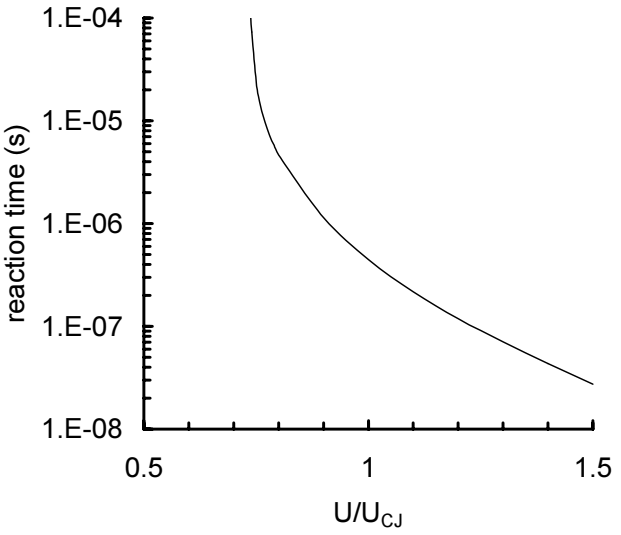

Figure 9. Reaction time behind shock waves in a stoichiometric hydrogen-oxygen mixture (P_o = 20 kPa) as a function of shock strength, U_{CJ} =2760 m/s.

is responsible for the failure of the detonation wave observed in Fig. 8b.

The decrease in shock strength in the diffracted region of the detonation can be understood by examining the analogous process in shock diffraction (Skews 1967). As shown in Fig. 10, diffraction around a sharp corner creates a self-similar, unsteady expansion fan that interacts with the shock. There is a distinct point at which the boundary of the disturbed region intersects the undisturbed shock front. Due to the diffracted front area increase and interaction with the expansion wave, the shock strength decreases continuously along the shock front from the boundary of the disturbed region up to the intersection of the diffracted shock with the side wall. The location of the boundary of the disturbed region on the shock can be determined by a simple acoustic construction (Fig. 11) that determines where the first disturbance from the corner intersects the incident shock wave.

From the geometry of this figure, the transverse speed V of the boundary of the disturbed region along the shock front is

$$V = \sqrt{c^2 - (U-u)^2} \tag{1}$$

where c is the sound speed behind the shock front, U is the shock speed and u is the postshock velocity in the lab frame. The trajectory of the disturbance boundary is a line with angle θ measured relative to the flow direction as shown in Fig. 1 . From the geometry of Fig. 11, this angle is

$$\theta = \tan^{-1}\left(\frac{V}{U}\right) \tag{2}$$

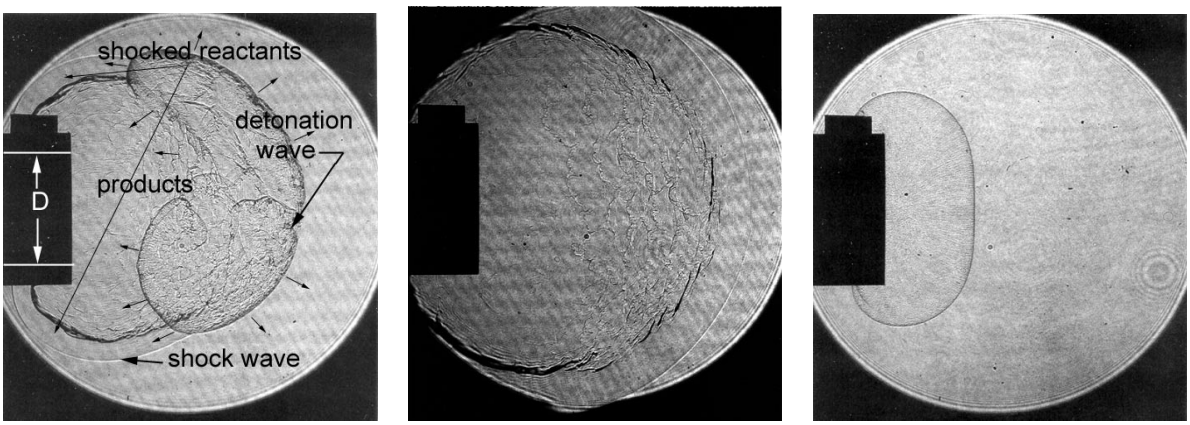

Figure 8. Shadowgraph visualization of the (a) critical (b) subcritical and (c) supercritical diffraction of a detonation wave emerging from a tube of diameter $D = 25$ mm into a large volume (Schultz 1998).

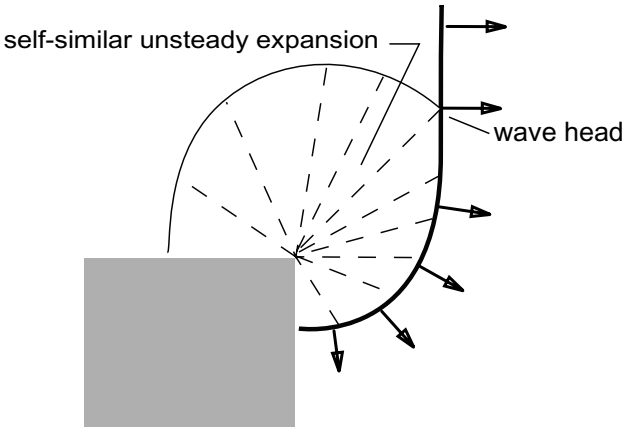

Figure 10. Region of similarity solution for shock diffraction around a sharp corner.

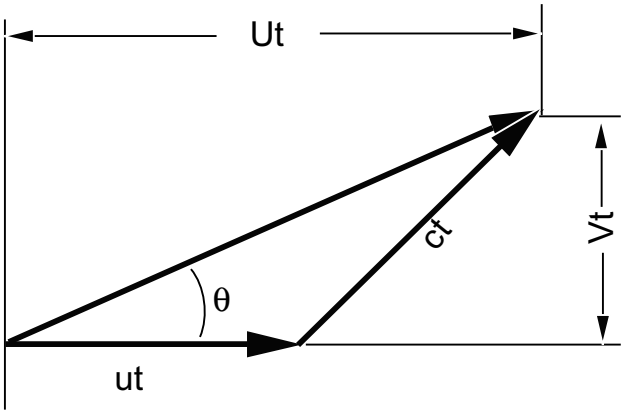

Figure 11. Skews' (1967) construction for determining the location of intersection of the disturbed region with the incident shock front in corner signalling problem.

The shock jump conditions can be used to evaluate the speed V and angle θ as a function of the incident shock speed. The results of calculations for a perfect gas are shown in Fig. 12. These computations indicate that the disturbance spreads at a finite rate that depends on the shock Mach number and ratio of specific heats. For large shock Mach numbers, $M_s > 5$ to 7, typical of detonation fronts, the angle asymptotes to a value between 15 and 30 degrees for $1.1 < \gamma < 1.67$. Observations of diffracting shock waves (Skews 1967) agree with these predictions.

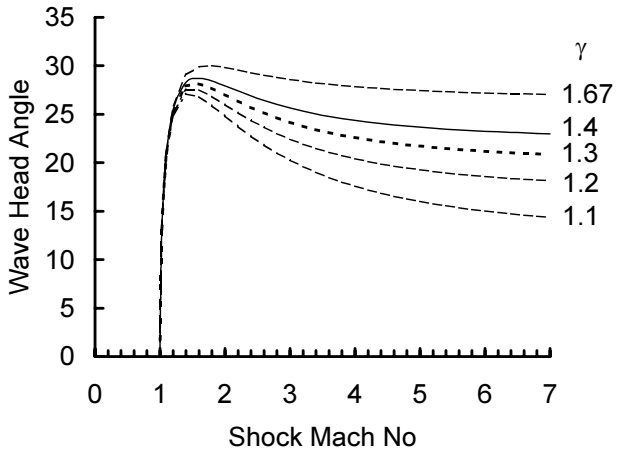

Figure 12. Disturbance angle computed using Skews' construction for a shock wave in a perfect gas, no reaction.

The propagation of disturbances and the magnitude of the disturbance speed play a key role in determining the critical condition in the detonation diffraction problem. Similar computations can be made for a detonation on the basis of assuming an infinitely thin reaction zone. This implies evaluating the sound speed and particle velocity at the product thermodynamic state found at the end of the reaction zone. The results are shown in Fig. 13 for the stoichiometric hydrogen-oxygen case and the shock wave results are shown for comparison. Inspection of this figure reveals that for a detonation traveling at the CJ speed, the transverse signalling wave speed based on the equilibrium prod-

uct state is zero, i.e., $\theta = 0$. This leads to a paradox first articulated by Gvozdeva (Bazhenova et al. 1965) that CJ detonations should diffract without any influence of the diffracting aperture size.

However, our observations and those of previous researchers (Bazhenova et al. 1965, Edwards et al. 1979, Zeldovich et al. 1956) indicate that not only does the aperture size have a strong influence on the diffraction but also the signalling speed V is clearly finite. The resolution to this paradox is to consider the role of the reaction zone structure (Fig. 3) in the signalling problem. The results shown in Fig. 13 indicate that there must be a continuous variation of transverse signalling speed between the shock and the end of the reaction zone. This arises because of the variation in the thermodynamic state and velocity through the reaction zone. The idealized one-dimensional approximation to a detonation (ZND model) has been used to evaluate the variation of transverse signalling speed and a representative result is given in Fig. 14.

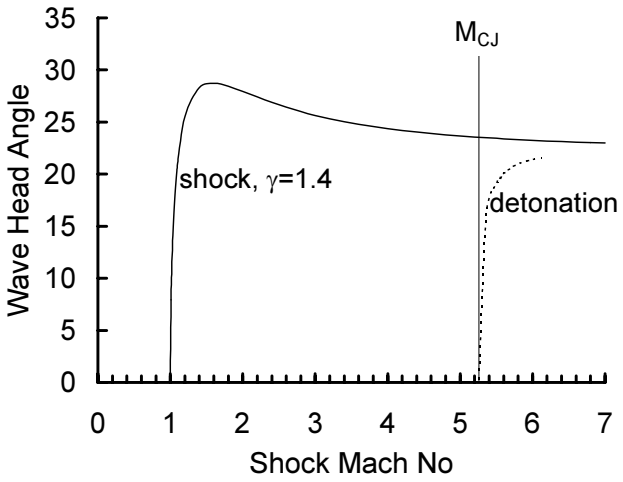

Figure 13. Disturbance angle computed using Skews' construction for leading shock wave and the detonation products for a stoichiometric hydrogen-oxygen mixture ($P_o = 20$ kPa).

Note that the signaling speed in Fig. 14 has a maximum value close to the shock front and that the maximum signalling speed can be approximated by the value at the front. This suggests that the results of Fig. 12 can be used to estimate that rate at which the disturbance propagates into the front. Signalling within a reaction zone is a complex problem (Barthels and Strehlow 1966) since the sound speed and fluid velocity depend on position. However, in the present analysis, we are only concerned with how the leading disturbance propagates. For the case of the stoichiometric hydrogen-oxygen mixture, this is about 1200 m/s, resulting in a signalling boundary angle of about 23°. Experiments are in progress at our laboratory to make measurements of the disturbance propagation in a variety of mixtures.

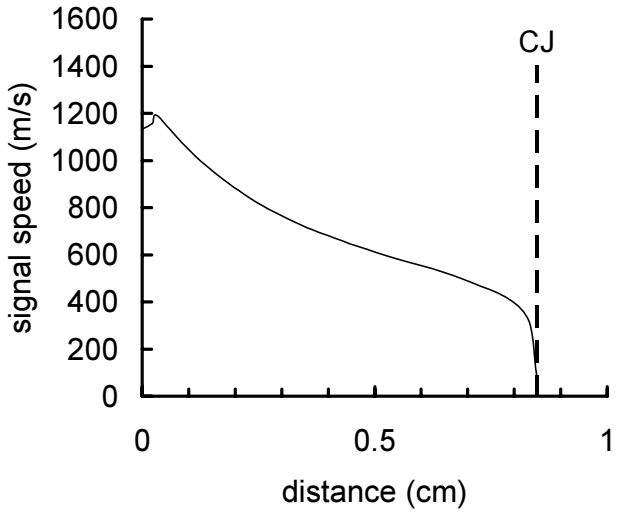

Figure 14. Signaling speed computed using generalization of Skews' construction for detonation reaction zone region, CJ detonation in stoichiometric hydrogen-oxygen mixture ($P_o = 20$ kPa).

The signalling process and the propagation of disturbances along the detonation are the easiest understood aspects of the diffraction process. Much more challenging are the phenomena shown in Fig. 8a, in which the disturbance initiates the failure of the detonation and then at some point, a spontaneous reemergence of the detonation occurs. The process of failure can be readily explained through the combination of the dependence of the reaction zone length on shock strength (Fig. 9) and the rapid decrease in shock strength from the disturbance head to the wall. However, additional considerations are needed to describe the re-emergence of a detonation since only a monotone increase in reaction zone length is predicted with decreasing shock strength. This problem is very closely related to that of detonation initiation by spherical shock waves in which a critical energy level is observed for initiating detonations. That critical energy level is apparently a consequence of a second time scale associated with a critical level of unsteadiness (Eckett et al. 1998) that determines if reactions will be quenched or continue to propagate. Similar considerations should apply to the critical tube problem and work on these ideas is in progress.

4. Summary

Chemical reactions lead to the breakdown of self-similar behavior in diffracting detonation and shock waves. Experimental observations of detonation diffraction around convex and concave corners show

that this occurs in a distinct fashion for these two cases.

In the case of diffraction around a concave corner or Mach reflection, the phemonena are superficially similar to those of nonreactive shocks, exhibiting simple Mach reflection for small ramp angles and regular reflection for large angles. However, for small ramp angles, the triple point is diffuse, apparently because the reflected wave strength is comparable to that of the transverse waves. An alternative explanation is that the reflected wave is a compression wave of finite thickness due to the reaction zone thickness. The diffraction process appears to be self-similar in the limit of very large or very small Mach stems as compared to the detonation cell width (or reaction zone length). The trajectory of the triple point is bounded by the limiting cases of frozen and equilibrium behavior. As a consequence, experiments with differing reaction zone lengths will result in different outcomes for both the triple point trajectory and transition point between regular and Mach reflection. This can help explain the discrepancies between experiments carried out with different fuel-oxidizer systems.

In the case of diffraction around a convex corner, a detonation can fail during the diffraction process. Detonation failure is apparently a consequence of unsteadiness quenching the reactions in the expansion wave that is produced by the flow around the corner. Failure of the detonation means that the front separates into an essentially non-reactive shock wave followed by a contact surface that may evolve into a flame. When the diffraction occurs through a channel or tube, complete failure is only observed when the tube or channel width is smaller than some multiple of the detonation cell width. Near the critical condition a detonation wave spontaneously re-emerges within the partially quenched reaction zone. The mechanism and prediction of this re-emergence of a detonation is one of the key unsolved problems in detonation physics today. We are focusing on explanations that involve signal propagation within the reaction zone and critical levels of unsteadiness competing with reaction processes.

Acknowledgement. This work was partially supported by the Powell Fund of the California Insitute of Technology and a NASA STTR contract in collaboration with Advanced Projects Research Inc., La Verne, CA.

References

Akbar R (1991) On the Application of Whitham Theory to Detonations. MS Thesis, Rensselaer Polytechnic Institute, Troy, NY.

Akbar R (1997) Mach Reflection of Gaseous Detonation, Ph.D. Thesis, Rensselaer Polytechnic Institute, Troy, NY.

Barthels HO, Strehlow RA (1966) Wave propagation in one-dimensional reactive flows. *Phys. Fluids* **9**, 1896-1907.

Bazhenova TV, Gvozdeva LG, Lobastov Y, Naboko IM, Nemkov RG (1965) *Shock Waves in Real Gases*, Nauka Press, USSR.

Eckett CA, Quirk JJ, Shepherd JE (1998) An analytical model for direct initiation of detonation. *Proceedings of 21st ISSW*, Eds. Houwing et al., Vol I, 383-388.

Edwards DH, Thomas GO, Nettleton MA (1979) The diffraction of a planar detonation wave at an abrupt area change. *J. Fluid Mech.* **95**, 79-96.

Edwards DH, Walker JR, Nettleton MA (1984) On the Propagation of Detonation Waves Along Wedges. *Archivum Combustionis* **4**(3), 197-209.

Garilenko TP, Prokhorov ES (1983) Overdriven Gaseous Detonations. *Prog. Astro. Aero.* **87**, 244-250.

Hornung, HG (1985) Regular and Mach Reflection of Shock Waves *Ann. Rev. Fluid Mech.* **18**, 33–58.

Hornung HG, Smith GH (1979) The influence of relaxation on shock detachment. *J. Fluid Mech.* **93**, 225-239.

Meltzer J, Shepherd JE, Akbar R, Sabet A. (1993) Mach Reflection of Detonation Waves. *Prog. Aero. Astro.* **153**, 78-94.

Schultz E (1998) Unpublished results. Graduate Aeronautical Laboratories, California Institute of Technology, Pasadena, CA.

Skews, BW (1967) The shape of a diffracting shock wave. *J. Fluid Mech.* **71**, 769-784.

Shepherd JE, Moen IO, Murray SB, Thibault PA (1986) Analyses of the Cellular Structure of Detonation. *21st Symp. (Intl) Combust.*, 1649-1658.

Zeldovich YB, Kogarko SM, Simonov NN (1956) An experimental investigation of spherical detonation in gases. *Sov Phys. Tech. Phys.* **1**, 1689-1713.